Chapter 11
Electronic Properties of Metal/Organic Interfaces

Christian Loppacher

Abstract A detailed understanding of the interface dipole formation between organic molecules and metal electrodes is a key issue for the fabrication of organic devices. This chapter will give an overview of the work done in this field. A comparison of macroscopic methods and KPFM, both used for the characterization of the electronic properties of molecular assemblies on these surfaces, will show that KPFM is capable of revealing the same quantitative results, however, with a nanometer scale resolution. Several examples will be used to point out the importance of exactly knowing the nanoscopic organization and orientation of these molecular assemblies to be able to fabricate reproducible devices with a few or even single molecules.

11.1 Introduction

Nowadays, thin films of organic molecules are widely used for the fabrication of macroscopic devices such as light emitting diodes (LED), solar cells, and chemical sensors, to name only a few. Smaller elements like organic field-effect transistors (OFET) or even single molecular devices with various functionalities are explored in research and are already working on test benches (for an overview in organic electronic devices see [1] and references therein). A key issue in all of these applications is the control of the electronic properties at the metal/organic interface which, of course, first needs a detail understanding of the processes involved.

C. Loppacher (✉)
Aix-Marseille Université, IM2NP, Centre Scientifique de Saint-Jérôme, Avenue Escadrille Normandie-Niemen, Case 151, 13397 Marseille CEDEX 20, France

CNRS, IM2NP (UMR 6242), Marseille-Toulon, France
e-mail: Christian.Loppacher@im2np.fr

S. Sadewasser and T. Glatzel (eds.), *Kelvin Probe Force Microscopy*, Springer Series in Surface Sciences 48, DOI 10.1007/978-3-642-22566-6_11,
© Springer-Verlag Berlin Heidelberg 2012

Organic materials have a wide band gap (2–3 eV) and a small thermally excited carrier concentration. Thus, a priori, Fermi level (E_f) alignment and band bending as observed at semiconductor interfaces are not given. At many metal/organic interfaces, it is rather a dipole layer at the interface due to charge transfer, chemical reaction, or other charge rearrangements that dominates the interface properties (see, e.g., [2]).

Let us first address the question of what is desired for best device operation. In most electronic devices, a good ohmic contact with a low injection barrier height is required. Therefore, the metal electrode and the organic functional layer must be well chosen to provide the desired energy level alignment. The contact resistance depends on many factors such as the work function of the metal electrode used, the properties of the organic material (ionization potential, IP; electron affinity, EA; etc.), and of course on the interface properties (vacuum-level shift, band bending, and interface-dipole formation) [3]. Therefore, device-specific tailoring of metal/organic interfaces is addressed in many studies. Solutions for selected metal/organic contacts are presented, and systematic studies were performed to choose the combination of metal electrode and organic material which would give the best performance. For multilayer devices such as solar cells, it is not only the contacts but rather the gradient of the built-in potential within the space charge layer (band bending in thicker region) which is crucial for optimizing the efficiency of charge separation. In this chapter, we will not address the problems that arise in doped organic multilayer devices but rather the effects that occur at the direct metal/organic contact.

The effects that occur at metal/organic interfaces are manifold and can often not be regarded as isolated problems. A few are more substrate related and may occur as a modification of the metal work function (ϕ_m). ϕ_m can change as a result of surface rearrangements or screening due to mirror charges. Some other effects are more adsorbate related. For example, band bending within the organic adsorbate layer was observed to be both gradual and linear [4], intermolecular interaction can lead to depolarization due to neighboring molecules, or molecular assembly. The latter can influence the interface properties as a function of molecular conformation or orientation, of order and disorder, of packaging density, but also due to defects in films and grain boundaries. Most of the named effects depend on both substrate and adsorbate as for example also chemical binding or dipole formation.

From an electronic point of view, all the above-described effects will lead to the formation of different types of contacts: an ohmic contact, a Schottky–Mott contact, or the dipole formation at the interface, for example. In many cases, a clear separation between these types of contacts is not possible since for the same materials of electrode and organic material, it can depend on many factors such as the film thickness, the structural arrangement of the organic material, and many more.

11.1.1 Ohmic Contact

Low-resistance, stable contacts are required at the interface of organic electronic devices. An ohmic contact is both linear and symmetric in its current-voltage characteristics. In a simple picture, electrodes made from metals whose work function is close to the organic adsorbate electron affinity (EA) should most easily form ohmic contacts. As mentioned above, the contact resistance depends on the details of the interfacial chemistry. Therefore, chemical reaction and surface reconstruction are some of the factors that make the reproducible formation of ohmic contacts challenging.

11.1.2 Schottky–Mott Contact

The Schottky–Mott contact is a textbook model for a semiconductor/metal interface [5, 6]. In a semiconductor, conduction and valence bands as well as a well-defined forbidden energy gap are formed. Electrons are free to move throughout the solid and thermal equilibrium is achieved. The Schottky–Mott model assumes common vacuum level (VL) and alignment of the Fermi levels E_f as a result of band bending at the semiconductor/metal interface. Its current-voltage characteristic is nonlinear and asymmetric; it has rectifying properties similar to semiconducting p-n junctions. In the case of organic material with a wide gap in the order of 2–3 eV and thus larger than the thermal energy, the concentration of thermally excited carriers is extremely small. Therefore, thermal equilibrium with E_f alignment and band bending in the organic layer close to the organic/metal interface cannot be assumed a priori. Especially for thin organic layers, it is mostly the vacuum level shift (dipole formation) at the interface described in the following that dominates the electronic properties for charge carrier injection.

11.1.3 Dipole Formation at Interface

As mentioned above, a common VL at organic/metal interfaces is often not achieved, but rather a VL shift leading to the formation of an electric dipole layer Δ. This layer can safely be assumed to be a pure interface property concentrated to a single or very few monolayers only; it is a consequence of a lack of mobile charge carriers in the organic material. For thicker layers, it often occurs in combination with band bending and E_f alignment [7].

The origins for this dipole layer formation are manifold: polarization of molecules, charge transfer across the interface, charge rearrangement or redistribution of the electron cloud [8], interfacial chemical reaction (chemisorption), dipole alignment, pillow effect and image forces, and many more. In the case of organic

molecules, these properties show a strong dependence on molecular ordering, packaging density, defects, molecular conformation, adsorption sites, to name only a few. Thus, for a detailed understanding of the interface properties, macroscopic methods must be complemented with nanoscale investigations to exactly determine all nanoscale geometrical and electronic parameters.

11.1.4 Macroscopic Methods

Up to now, most systematic studies (see Sect. 11.2) on the organic/metal interface have been performed with macroscopic methods such as the Kelvin Probe (KP), photoelectron spectroscopy (PES) and in special UV photoelectron spectroscopy (UPS), or inverse photoelectron spectroscopy (IPES). All the above-mentioned methods either use the emission of electrons or they rely on well-conducting samples. Therefore, for organic/metal interfaces that often have a reduced conductivity, their application must be done very carefully. In the following sections, IPES, PES, and the KP method will briefly be discussed including the different properties that can be retrieved from these techniques.

11.1.4.1 Kelvin Probe

The macroscopic Kelvin Probe (KP) was developed by Lord Kelvin in 1898 [9]. As depicted in Fig. 11.1a, two plane electrodes of metals with different work function ϕ_1 and ϕ_2 are placed close and parallel to each other to form a capacitor. When the electrodes are connected, Fermi level E_f alignment is achieved and a voltage:

$$V = \frac{\phi_1 - \phi_2}{e}$$

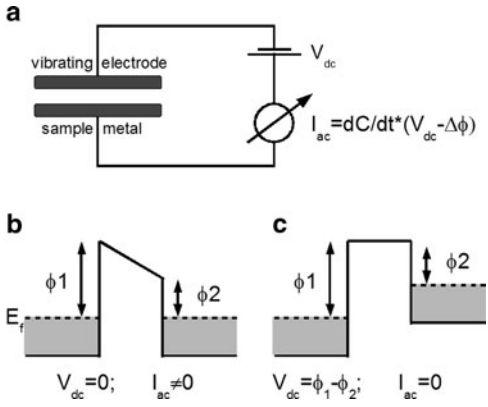

Fig. 11.1 (**a**) A metallic sample surface and a plane electrode are connected with a *dc*-voltage source as well as a current meter. (**b**) Mechanically vibrating the electrode will create a displacement current I_{ac} when $V_{dc} = 0$. (**c**) I_{ac} can be nullified by compensating the contact potential difference V_{CPD} by applying $V_{dc} = \phi_1 - \phi_2$

corresponding to the work function difference between the two metals is built up across the capacitor as it gets charged by the displacement current (Fig. 11.1b). e is the elementary charge of an electron. The total charge Q in the capacitor is $Q = C \cdot V$. It depends on the capacity of the plate capacitor $C = \varepsilon \cdot A/d$ with the permittivity ε, the surface of the plates A, and the distance d between them. As C is a function of the distance d, it varies when d is modulated as a function of time. As a result, the charge is modulated which leads to an ac-displacement current $I_{\mathrm{ac}} = \mathrm{d}Q/\mathrm{d}t$. The latter is measured and can be nullified when an additional dc-voltage equivalent to $-V_{\mathrm{cpd}}$ is added in the circuit to make the voltage across the capacitor $V = V_{\mathrm{cpd}} + V_{\mathrm{dc}} = 0$ equal to zero (Fig. 11.1c). Thus, KP nullifies the displacement current between two metal plates by applying an appropriate V_{dc} which gives a direct measure for the work function difference between the two electrodes. If one electrode is made of an inert, well-defined metal with calibrated work function, quantitative results are obtained. KP integrates over the size of the electrodes; although it relies on measuring a current, it has been shown that it correctly maps the surface potential also for poor conducting surfaces [4, 10].

11.1.4.2 Photoelectron Spectroscopy

PES uses a monochromatic photon source to illuminate the sample surface [11, 12]. For UPS, most instruments use gas discharge lamps with an energy of either 21.2 eV (He-I) or 40.8 eV (He-II). These energies are sufficient to emit electrons from occupied states due to the photoelectric effect. The energies of these emitted electrons are analyzed with a spectrometer to determine their original electronic state in the solid. Electrons emitted from the surface escape from the topmost layers with a depth of a few nanometers only, and thus UPS is very surface sensitive.

For metallic surfaces, the electrons with the highest kinetic energy in the analyzer originate from the Fermi level E_f and can be used to calculate the work function ϕ of the sample. Using careful analysis for increasing film thicknesses, further organic/metal interface properties such as the vacuum level (VL) shift relative to the substrate E_f (dipole formation), or the ionization potential (IP) can be determined.

11.1.4.3 Inverse Photoelectron Spectroscopy

Inverse PES (IPES) is a complementary method to PES to gain information on the empty states of the surface. In IPES, the sample surface is exposed to an electron beam and the emitted photons are analyzed in energy. The energies of the emitted photons are characteristic for the decay processes of the incident electrons into all of the unoccupied electronic states below their initial energy. In such a way, IPES will give a picture of the unoccupied electronic states above E_f. Especially, the electron affinity (EA) or the position of the lowest unoccupied molecular orbital (LUMO) can be estimated. The incident electron beam has a very low penetration depth; thus IPES is sensitive to a few atomic layers only.

For organic material especially with low conductivity, PES and IPES must carefully be evaluated since charging of the surface and final state screening can influence the energy of emitted or collected electrons. Furthermore, radiation damage can make it impossible to apply these methods for certain materials.

11.1.5 Nanoscopic Methods: Kelvin Probe Force Microscopy

In the past years, many techniques based on scanning force microscopy (SFM) have been developed to investigate electronic properties on the nanometer scale (for an overview, see, e.g., [13]). Conducting probe SFM [14], scanning capacitance microscopy [15], electrostatic force microscopy (EFM) [16], and Kelvin probe force microscopy (KPFM) [17, 18] (KPFM) have been developed and can be used to measure the properties such as current flows, resistance, capacitance, electrostatic forces, charge distribution, surface potential, and voltage drops on the nanometer scale. All of these SFM-based methods can provide simultaneous topographic imaging. The lateral resolution achieved, however, depends on the probes used as well as the distance between tip and sample during the measurements.

For imaging surface potentials or charge distribution, local work function, and electrostatic forces, KPFM is the method which provides the best spatial resolution. The details on the physical effects that determine the imaging process in KPFM and on how exactly the method can be implemented are described elsewhere (see Chap. 2). Here it is just reminded that the imaging process of KPFM relies on minimizing the electrostatic force or its gradient between the tip and the sample by applying an appropriate *dc*-voltage V_{dc} between tip and sample. The measured value of V_{dc} corresponds to the local contact potential difference (LCPD). In order to extract quantitative values out of the acquired signal, either areas on the surface or a well-characterized tip have to been taken for calibration (e.g., with known work function). Although KPFM can be used to measure the LCPD on even an atomic length scale (see Chap. 13), its quantitative resolution is in the order of the diameter of the tip front end. Note that KPFM is fundamentally different from macroscopic Kelvin Probe (KP) in which a current is nullified and hence conducting samples are needed. KPFM perfectly works for poorly conducting organic material or for insulating samples; however, charging can lead to an offset of the measured local values.

11.2 Macroscopic Studies

The macroscopic characterization methods described above have been intensively used to characterize the organic/metal interface to gain insight into the details of the contact formation of organic layers to metallic electrodes.

One large group of studies is focussing on the organic/metal interface for rather thick organic layers and is discussing mostly the effects of band-bending, interface dipole formation, as well as the Fermi level alignment at these interfaces. PES and the macroscopic Kelvin Probe (KP) are used to investigate the properties of these interfaces. A general review on the electronic properties at organic/metal interfaces is given by Ishii et al. in [19]. For the KP, it has been stated that it is well suited to measure Fermi level shifts at organic/metal interfaces, and that Fermi level alignment is not achieved in many cases [7, 10, 20] due to the formation of an interface dipole layer. Furthermore, for increasing thicknesses KP can be used to observe band bending or effects due to screening [4]. The conclusion that Fermi level alignment is not always achieved is supported by various PES studies which can give a little more insight into the details of the interface properties. For example, it has been shown that the interface dipole is confined to a few nanometers only, and that it linearly depends on the difference between the ionization potential and the transport gap in the case of phthalocyanines with different degree of fluorination [21, 22]. In these studies, besides the formation of a dipole layer, different contributions are identified which are responsible for the potential drop at the interface: modification of metal work function (mirror force or surface rearrangement) and potential drop in the organic layer (band bending).

Other studies focus more on the very first layer of an organic material adsorbed on metal surfaces. For example, it has been shown by KP that Ag electrodes can be chemically tailored via the adsorption of different self-assembled monolayers (SAM) to control the electronic interface properties of organic diodes [23]. Various studies have been performed to measure the work function change of metals upon deposition of organic layers [7], in many cases, a linear dependence between the metal work function and the interface dipole is found [2, 20, 24]. Both positive and negative dependencies are found. For most systems studied, the interface dipole is confined to the very first layer. However, the strength and the orientation of the dipole depend on various parameters. For example Venkataraman et al. [25] used different alkanethiols to tune surface chemical gradients by changing the coverage, the orientation, or the component gradient. The observed shifts in binding energy are due to interface charge redistribution, surface coverage, chemical nature, and molecular orientation. For monolayer SAM, the electronic interface properties can be tuned using different alkanethiols with either different terminal groups [26] or different chain lengths [27]. Also, the side groups of porphyrin molecules can change the work function shifts on various metal surfaces as demonstrated by Alkauskas et al. [28]. Furthermore, De Renzi concludes that the molecular level alignment is influenced by the value of the local work function, which in real, inhomogeneous surfaces, substantially differs from the typically measured average value [29]. One other effect is spontaneous dipole alignment which can occur for multilayers of polar molecules such as N_2O [30] or Alq_3 on gold [31]. In the latter study, the aligned dipoles formed a giant surface potential of several tens of volts.

In summary, the most prominent effects at the interface of ultrathin organic films with a metal substrate are the following: Fermi level alignment is not necessarily achieved but rather a dipole layer at the interface is formed. In most cases, this layer

is confined to the very first monolayer only. Furthermore, the size of the dipole layer often linearly depends on the metal substrate work function. Theoretical studies can be used to identify the origins of the dipole formation. For example at the Alq_3/Al interface: (1) charge transfer, (2) mirror force, (3) push back effect due to Pauli repulsion between metal and molecular electrons, (4) chemical interaction, (5) interface state, and (6) permanent dipole of adsorbates are determining the dipole formation [32]. It is therefore not always the direction of a charge transfer that determines the orientation of the dipole, but rather the redistribution of the electronic cloud as a function of the above-mentioned effects [8].

In most of the above-mentioned macroscopic studies that investigate the origin of the interface dipole formation, it is pointed out that it is crucial to exactly know the substrate surface reconstruction, the precise adsorption site of the molecule, its conformation as well as the intermolecular assembly. These nanoscale geometrical information in combination with the local electronic properties can be acquired by noncontact atomic force microscopy (nc-AFM) in combination with KPFM.

11.3 Nanoscopic Studies

KPFM can be used to measure many electronic properties such as local dopant concentrations [33, 34], surface charging due to photoinduced charge separation [35–37], interface dipole formation between a metal surface and an organic layer [38, 39], or an ionic thin film [40], electronic band bending at semiconducting interfaces [41–46], contrast due to differently terminated or reconstructed surface orientations on the facets of a nanocrystal [47], at grain boundaries [48], and on ordered and disordered surfaces [49], to name only a few of the first experimental results. These examples show that the contrast provided by KPFM reveals important information in addition to the sample surface topography.

11.3.1 Quantitative Results by KPFM

As mentioned in Sect. 11.1.5, for a quantitative interpretation of the measured KPFM contrast, the tip work function must be known. Furthermore, although nanoscale information is obtained, a quantitative interpretation is only valid if either the observed nanoscale object is larger than the tip front end or if quantitative values can be obtained by comparing the measured data with the results obtained from KPFM image simulations using effective tip geometries and optimizing the local CPD distribution [50–53].

For ultrathin alkali halides on metal surfaces [51] as well as for C_{60} molecules on various metal substrates [54], it has been shown that KPFM reveals quantitative values on a nanometer scale that are in agreement with the macroscopically acquired results by UPS and KP.

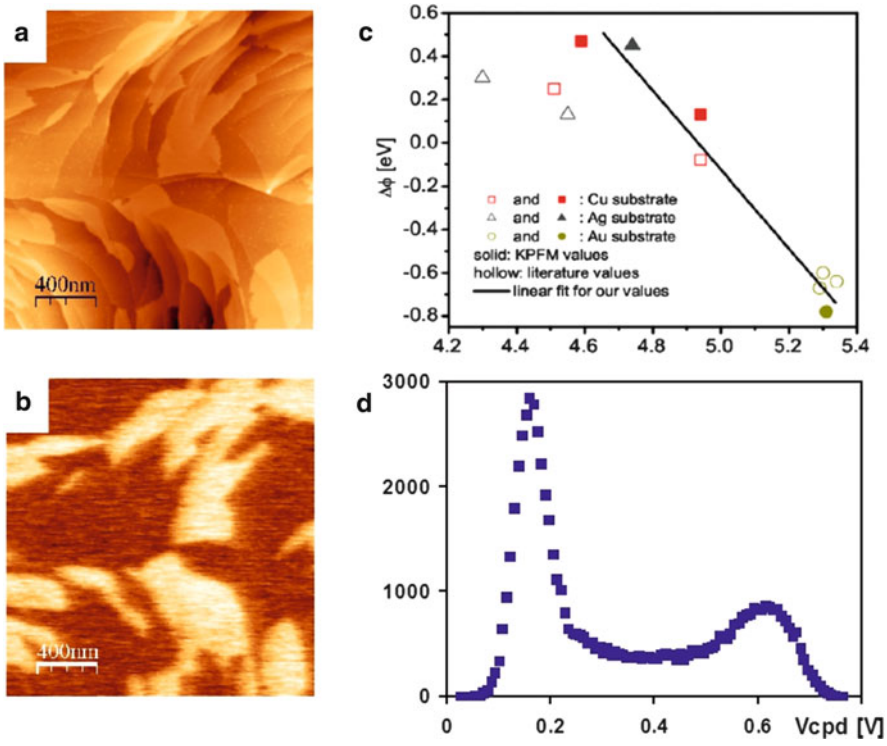

Fig. 11.2 (**a**) NC-AFM topography image (2 × 2 μm, *z*-scale 1 nm) and (**b**) simultaneously recorded KPFM signal of 0.5 monolayer C_{60} on Ag(111). (**c**) Overview of different experimental results for work function changes of clean metal substrates after deposition of C_{60}. (**d**) Histogram of the values recorded in (**b**), the distance between the two peaks corresponds to a work function change of $\Delta\phi = +0.45$ eV [54]

In the latter study by Zerweck et al. [54], the adsorption of C_{60} on various metal substrates was investigated by KPFM. C_{60} is a molecule widely used for different applications in organic electronic devices, and furthermore, C_{60} can be used to tune the interface properties between a metal substrate and an organic layer [55–57]. The KPFM experiments for Ag(111), Au(111), Cu(100), and Cu(111) single crystal substrates by Zerweck et al. were measuring the work function difference between the metal substrate and one monolayer thick islands of C_{60} on only partially covered samples (Fig. 11.2).[1] Figure 11.2a, b shows the topography and the Kelvin signal, respectively, for the Ag(111) surface partially covered with C_{60}. The clear Kelvin contrast in Fig. 11.2b can be evaluated by taking a histogram of the voltages applied by the KPFM as depicted in Fig. 11.2d. Triple-Gaußian[2] peak fitting reveals the

[1] For image evaluation, WSxM [58] was used.

[2] The third peak is used to account for the background noise.

distance between the two peaks which for the present example corresponds to the contact potential difference (CPD) (V_{CPD}) between the pure Ag(111) surface and the areas covered by 1 ML of C_{60} ($\Delta\phi = +0.45$ eV). The calibration of the data was done by taking the work function for the pure Ag(111) substrate from literature [59] as a reference which is then attributed to the value measured for the pure Ag(111) substrate. The results for all investigated metal surfaces are displayed in Fig. 11.2c where they are compared to the values obtained macroscopically by KP and by UPS [20, 60–63]. The scatter of the values for the bare metal work function for copper and silver might be due to the fact that these surfaces are not that noble and tend to react with residual gases present even in ultrahigh vacuum (UHV). All the same, this study showed that, first, nanoscale KPFM experiments are in very good agreement to the macroscopically acquired ones, second, what is valid for most organic molecules physisorbed on metal substrates: the interface dipole layer which is formed linearly depends on the substrate work function (see Sect. 11.1.3), and third, quantitative resolution in KPFM can be obtained on a length scale as small as 10 nm. This high resolution was achieved when using ultra sharp well-conducting AFM tips that were covered with an ultrathin chromium layer [54].

Different nanoscale KPFM studies support the importance of exactly knowing the geometrical and chemical properties of the investigated organic/metal contacts since many parameters can change the strength or even the direction of the interface dipole. Cui et al. [64] showed that the interface dipole layer at carbon nanotube/Au contacts can reversibly change its direction as the environment changes from air to vacuum or an oxygen-free environment. Miyazaki et al. [65] observed that the structural order of methylquinquethiophene (M5T) strongly influences the electrical resistance of the film. Furthermore, these authors observed the formation of a first monolayer of M5T on platinum electrodes with a hight resistance, higher than the one observed for example at grain boundaries. Yamada et al. [66] studied layers of organic molecules on Pt substrates. Different surface potentials were observed for the first as well as the second monolayer. The authors explain these results by a charge transfer for the first monolayer and an induced polarization for the second one. Finally, the dipole moment normal to the substrate obtained by ab initio MO (molecular orbital) calculations were also used to predict the surface potentials of patterned SAM [67].

Besides these studies of organic layers directly adsorbed on metal substrates, there have also been a few reports on KPFM applied to organic material on insulating substrates. Palermo et al. [68] report on acceptor–donor phase segregated blend films adsorbed on mica. In these films, each component clearly possesses significantly different nanoscale electronic properties from its neat film. This is due to molecular ordering as well as due to the interaction between the two components. The molecular ordering and orientation with respect to the substrate also influenced the CPD measured for PTCDA on ultrathin KBr films on Ag(111) as observed by Loppacher et al. [69] (see Sect. 11.3.2). In other experiments, Glatzel et al. [70] measured a clear contrast in the KPFM signal between molecules and gold nanoclusters on the insulating surface of KBr. The contrast formation is explained by variations of the local surface potential or the local dipole moment.

In the following, some examples will be discussed where either the orientation of the adsorbed molecules with respect to the surface or their organization on the surface influence the measured CPD. All investigated samples were prepared under UHV conditions and measured in situ with a commercial low-temperature AFM (Cryogenic SFM Omicron Nanotechnology GmbH) at 80 K.

11.3.2 Orientational Dependence

The first example we are going to discuss is the adsorption of PTCDA (3,4,9,10-perylene-tetracarboxylic-dianhydride) on partially KBr covered Ag(111) [69]. The aim of this work was to use an ultrathin insulating layer (KBr) between the metal substrate and the organic molecules to control the vertical interaction (adsorbate–substrate) and therefore to influence the growth mode of the organic adsorbates. It was shown that the delicate balance between adsorbate–adsorbate (lateral) and adsorbate–substrate (vertical) interactions is indeed strongly influenced by the ultrathin KBr layer leading to a completely different molecular arrangement of PTCDA on the first and the second monolayer of KBr. A similar conclusion was drawn by Ramoino et al. [71] for the adsorption of porphyrins adsorbed on NaCl layers with different thicknesses on Cu(111). Simulations of the results by Loppacher et al. [69] with an extended Ising-type model reproduced the experimental patterns very well, especially the size of the observed molecular aggregates corresponds to the experimental values. Apparently, small aggregates are formed when the vertical and lateral interaction are competing, and larger ones are formed as soon as one of the interactions dominates. Besides the different sizes, in the smaller aggregates PTCDA formed rods in which the PTCDA molecules were laterally π-stacked and in the larger aggregates planar growth with the π-orbital parallel to the surface was observed.

Figure 11.3a, b displays the topography and KPFM signal for PTCDA adsorbed on a one (upper left part) and two monolayer (lower right part) thick KBr film on the Ag(111) substrate. The separation between the two areas of 1 and 2 ML thick KBr underneath the molecules is indicated by the dashed line. The molecules adsorb in two different conformations in a planar geometry and in rods where the molecules are oriented perpendicular to the substrate. The KPFM contrast in Fig. 11.3b shows three different levels, the darkest color corresponds to the KBr covered Ag(111) substrate, the medium one corresponds to the conformation in rods, and the brightest one is measured above the molecules adsorbed in planar geometry on the ultrathin KBr film. A difference in approximately 0.1 V (lowering of the work function) was observed between each, the KBr covered Ag(111), the molecules adsorbed in a planar conformation on the thin insulating film, and molecules adsorbed in stacks. These values can be taken from the histogram of the measured CPD values (Fig. 11.3e). Figure 11.3c, d shows the formation in rods (topography) as well as the planar growth of PTCDA (dissipation image in the area depicted in Fig. 11.3a). Interestingly, there is PTCDA in rods on both the first and the second ML KBr

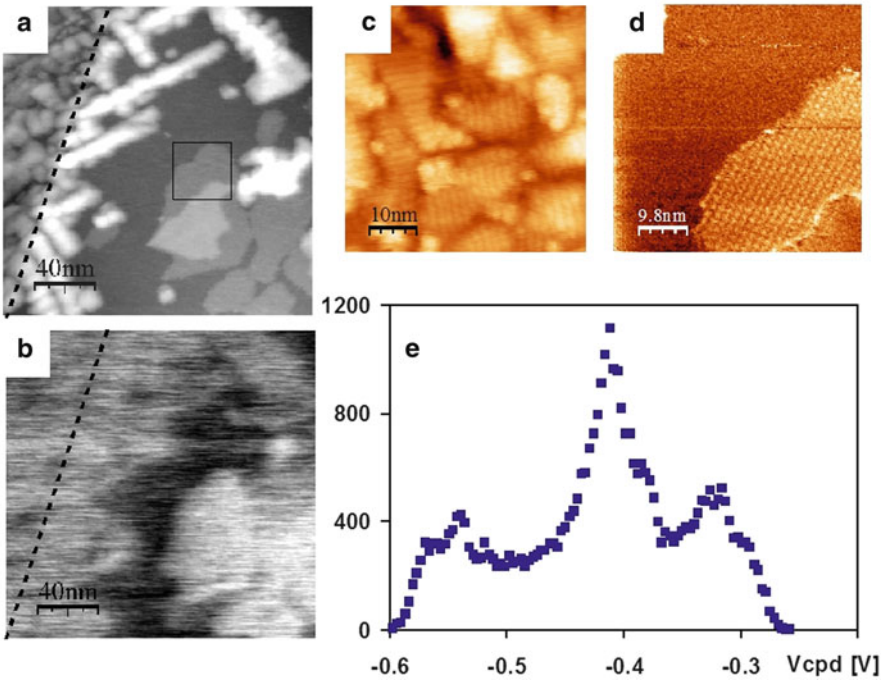

Fig. 11.3 (**a**) Topography (200 nm × 200 nm, *z*-scale 1.4 nm) of PTCDA on 1 ML (*upper left part*) and 2 ML (*lower right part*) of KBr/Ag(111). (**b**) KPFM image simultaneously acquired to the topography in (**a**) showing three different levels that are evaluated by the histogram displayed in (**e**). (**c**) and (**d**) show molecular resolution images for the two different assemblies found on this surface: (**c**) the formation of rods with the molecules π-stacked parallel to the surface (on 1 ML KBr/Ag(111), *z*-scale 0.5 nm), and (**d**) planar growth as observed mostly on 2 ML of KBr/Ag(111) (dissipation image) [69]

above which the CPD values are identical. Although, it is not the thickness of the underlying KBr film which determines the local CPD values but rather the orientation and the assembly of the molecules. A quantitative evaluation of the local work function can be made from the measured CPD values as follows: first, the work function of Ag(111) is taken from literature (4.74 eV [59]) and the work function difference between pure and KBr covered Ag(111) is measured before PTCDA deposition (−1.04 eV). This results in a reference value for the work function of KBr-covered Ag(111) of 3.6 eV. The PTCDA on KBr in rods increases this work function by ≈0.1 eV, and the PTCDA adsorbed in planar geometry increases the work function by ≈0.2 to an absolute value of 3.7 eV and 3.8 eV, respectively. These evaluations must be made with care, since due to the reactivity of the Ag(111) surface it is not guaranteed that after the deposition of KBr the work function of Ag(111) is not altered. Hence, taking literature values for metal work functions can lead to wrong absolute values; however, the measured local differences are correct.

The second example we will discuss is the adsorption of porphyrin molecules on highly ordered pyrolytic graphite (HOPG) [72]. Porphyrin compounds have been of interest for many years due to the facile ability to engender and tune optical and electrical functionality by varying the nature of the porphyrin ring central metal ion and modulating porphyrin σ- and π-system electronic structure through introduction of appropriate substituents at the macrocycle β- or meso-positions [73]. Many substituted porphyrin systems have been established to self-assemble on metal surfaces [74, 75]. Nikiforov et al. [72] deposited 0.6 monolayer (ML) of 5,15-bis (2′,6′-bis(3,3-dimethyl-1-butylocy)phenyl) porphyrin (compound **1**) [76] on the atomically smooth surface of HOPG.

Figure 11.4a depicts the resulting topography image which shows one part of a large island of porphyrin surrounded by the clean HOPG substrate. Typically, the molecules assembled in islands with sizes in the order of 1 μm; however, their

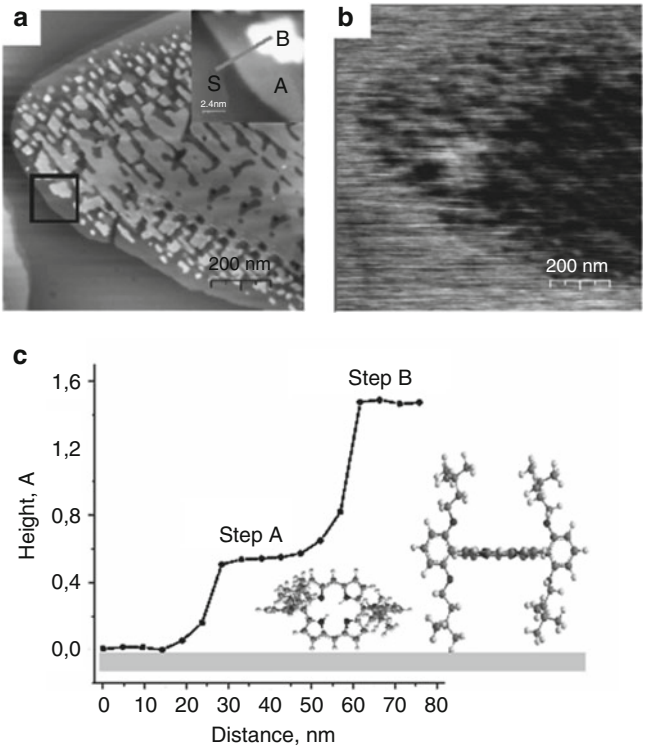

Fig. 11.4 (**a**) NC-AFM topography (*z*-scale 2.4 nm) and (**b**) KPFM image (*z*-scale 80 mV) (**b**) (1 μm × 1 μm) of 0.6 ML of porphyrin molecules adsorbed on HOPG. The inset in (**a**) shows a close up view of the topography image in the area indicated by the *black square*. A line profile drawn along the *gray line* marked in the inset is displayed in (**c**). A careful height analysis leads to the conclusion that in areas A the porphyrin ring is oriented perpendicular to the surface and in areas B with higher step height, the porphyrin ring is oriented parallel to the sample surface. In the latter case, there is a stronger dipolar coupling between the porphyrin ring and the surface [72]

organization was not homogeneous. What at first glance looks like a second ML of molecules which develops on the first one in the form of smaller islands is in fact a different conformation of the molecules in still the very first ML. A careful height analysis taken from the inset in Fig. 11.4a and displayed in Fig. 11.4c reveals two different step heights: 0.6 and 1.55 nm. The height of step A corresponds to the width of the porphyrin ring (∼0.7 nm), while that of step B matches the length spanned by the two 3,3-dimethyl-1-butyloxy groups which lie above and below the porphyrin plane. Both islands A and B are highly ordered, and an evaluation of their ordering using images with molecular resolution (not shown) reveals lattice parameters which confirm the following conclusions: The molecules in island A assemble with their porphyrin rings oriented perpendicular to the substrate, while in island B the porphyrin rings lie parallel to the substrate surface. These structures are similar to the "face on" and the "edge on" stacking modes of porphyrin molecules observed in monolayers and the solid state [77–80].

The interesting result of the above-described experiments is that there is a difference in the surface potential measured by KPFM for the two molecular arrangements. Figure 11.4b shows the KPFM signal simultaneously acquired to the topography signal displayed in Fig. 11.4a. For the island A with the porphyrin rings perpendicular to the surface, the molecular ML shows the same work function as the one above the clean HOPG substrate. However, for the molecular layer with the porphyrin rings parallel to the HOPG surface, the surface work function is lowered by ∼50 mV. This is due to the fact that when the porphyrin ring is parallel to the surface, the π-symmetric orbital of the porphyrin and underlying substrate facilitate charge delocalization. A comparison between the expected dipole moment calculated by a simple model and the dipole moment deduced from the measured work function difference (∼50 mV) leads the authors to the conclusion that significant charge screening occurs at the porphyrin–HOPG interface for the islands of type B. When the charge density of the porphyrin lies perpendicular to the surface (island type A), the magnitude of the dipolar interaction is diminished greatly and no measurable change of the surface potential is observed. This study indicates that in a metal-porphyrin-metal device configuration, molecules oriented with the porphyrin ring parallel to the surface will demonstrate an increased hole injection barrier with respect to analogous structures oriented perpendicular to the surface. Thus, differences in surface potential that derive from molecular configuration have important implications for molecular and organic electronics.

11.3.3 Dependence on Molecular Arrangement

As mentioned in Sect. 11.1, the effects that occur at metal/organic interfaces are manifold. Often, they are both substrate and adsorbate related as it is for example in the case of chemical binding or dipole formation. In the above-described experiments, the orientation of the adsorbed molecule's π-orbital with respect to the surface changes the local work function. Hence, for the investigated organic/metal

contacts, the charge injection barrier will strongly depend on the morphology at the interface. Different other parameters can influence the interface properties such as order and disorder, packaging density, but also defects in films and grain boundaries. In the following, we are going to discuss an example which shows that both the packaging density and an order–disorder transformation can vary the local surface potential.

Milde et al. [81] used KPFM to investigate the work function changes that are generated by the adsorption of different structural phases of octachloro zinc phthalocyanine ($ZnPcCl_8$) on Ag(111). Phthalocyanines are a common class of organic dyes used for applications in optoelectronic devices, but might equally be used in molecular electronic devices due to their chemical stability, self-assembly behavior, and electronic properties [82–84]. The latter can be modified by substitution of the eight hydrogen atoms with either electron donors or acceptors, or by complementation with different metal atoms or metal complex cores [21, 85]. Standard phthalocyanine is known to show a good self-assembly behavior, but in a subtle balance between intermolecular and molecule-substrate balance. In a study by Abel et al. [86], the intermolecular interaction of ZnPc was enlarged by substitution of hydrogen with halogenides, which lead to a more complex self-assembly behavior of the synthesized $ZnPcCl_8$ with different phases. Within the first ML $ZnPcCl_8$ on Ag(111), distinct structural phases were formed which could be attributed to the formation of 8, 4, and 0 intermolecular hydrogen–halogen bonds [87].

In the work by Milde et al. [81], 0.5 ML of $ZnPcCl_8$ were deposited on the clean Ag(111) surface, and the sample was cooled down to 80 K after 10 min to preserve a surface on which the phases P1 and P2 coexisted. Note that at room temperature, the organization of the molecules develops toward P3 via the gas phase [86, 87]. In P1, the molecules are arranged in a rhombic phase showing no hydrogen–chlorine bonds. P2 is an asymmetric phase with four intermolecular bonds. Typically, for a submonolayer coverage, the molecules are arranged in rather large, highly ordered ML thick islands. Most of these islands have smaller peninsulas which occur at a changed voltage in the KPFM signal compared to the mother island. Figure 11.5a, c depicts the topography and KPFM signal of such an area, where all the Ag(111) substrate, P1 and P2 are imaged. The identification of the phases P1 and P2 was done by images with molecular resolution (not shown). The measured lattice constants were in excellent agreement with the ones observed by Abel et al. [86]. The observed work function change between the Ag(111) and an ML of $ZnPcCl_8$ in phase P1 is $\Delta\phi_{P1} = -(103 \pm 22)$ meV and in phase P2 $\Delta\phi_{P2} = -(54 \pm 20)$ meV.

As mentioned in Sect. 11.3.1, taking as a reference the work function from literature of a surface which tends to react with residual gases is quite delicate. Therefore, the authors evaluated the difference between the two surface potentials acquired above the phases P1 and P2 $\Delta\phi_{21} = \phi_{P2} - \phi_{P1} = (49 \pm 22)$ meV. This measured value can be used according to Iwamoto et al. [88] to calculate a charge density difference between the two phases of $\Omega_{21,m} = (0.026 \pm 0.014)(e^{-1}nm^{-2})$. For comparison, the authors performed density functional theory calculations using SIESTA [89, 90] to deduce the molecular density in the different phases as well as

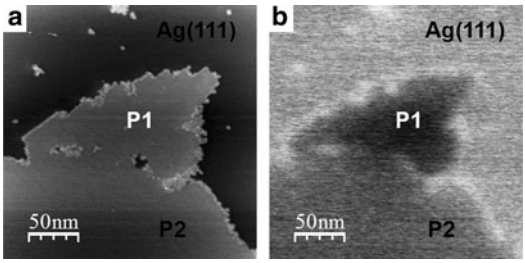

Fig. 11.5 (**a**) Topography (z-scale 0.8 nm) and (**b**) KPFM image (250 nm × 250 nm) of 0.5 ML $ZnPcCl_8$ adsorbed on the Ag(111) surface. Images with molecular resolution (not shown) were used to deduce the areas in which the molecules are organized in the rhombic phase P1 showing no hydrogen–chlorine bonds, and in the asymmetric phase P2 with four intermolecular bonds. The observed work function change between the Ag(111) and an ML of $ZnPcCl_8$ is $\Delta\phi_{P1} = -(103 \pm 22)$ meV in phase P1 and $\Delta\phi_{P2} = -(54 \pm 20)$ meV in phase P2 [81]

the charge per molecule. The latter is almost the same for all phases ($\sim 0.66\,e^-$ per molecule) and can be used with the molecular density to compute a charge density difference $\Omega_{21,c} = (0.033 \pm 0.002)(e^{-1}nm^{-2})$ which is well within the uncertainty of the one calculated from the measured values ($\Omega_{21,m}$, see above). Thus, the difference in work function measured by KPFM on these two differently assembled molecular layers can be attributed to a difference in charge density, which is a direct consequence of the intermolecular bonds.

Besides the difference in work function between highly ordered molecular layers of P1 and P2, there were also disordered layers that showed a much larger surface potential than the ordered ones. The size of disordered areas increased when the substrate temperature was increased during molecular deposition. Figure 11.6 shows an area with ordered (P1 and P2) and disordered (D) molecular layers as well as with pure Ag(111). The images in Fig. 11.6a, c were recorded before the images in Fig. 11.6b, d. Between the two, a scan in a smaller square area (indicated by the arrow) with increased tip sample interaction was performed. In the scanned area (40 nm × 40 nm), the slightly higher topography clearly shows that the molecules have undergone an order–disorder transition, and the KPFM signal shows an increased potential similar to the one observed in the disordered areas (D). In the disordered areas, it is most probable that the molecules are not adsorbed with their π-orbital parallel to the surface. The reversed sign of the work function change on disordered islands compared to the ordered ones indicates a completely different binding mechanism, since the symmetry of the molecule does not allow for a static dipole moment. Such a rise in work function upon $ZnPcCl_8$ deposition on Ag(111) was also observed by UPS [91]; however, in these experiments the ordering of the molecules is unknown and there might even be multilayer islands on the surface.

On the one hand, this order–disorder transition could be seen as a possibility for nanolithography; on the other hand, it shows how important it is to determine the exact morphology of the investigated samples on a molecular length scale. For $ZnPcCl_8$ on Ag(111) it is not only the density of the molecular assembly but also

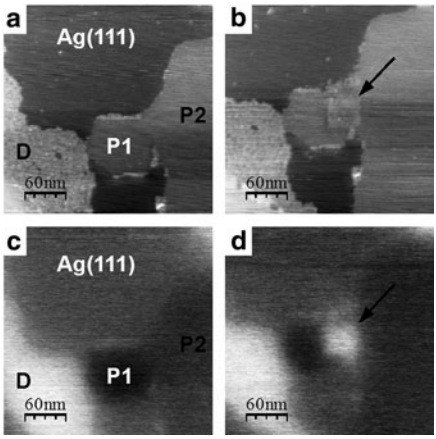

Fig. 11.6 (**a**) and (**b**) Topography (300 nm × 300 nm, *z*-scale 0.7 nm) and (**c**) and (**d**) corresponding KPFM images of 0.5 ML $ZnPcCl_8$ adsorbed on Ag(111). Areas of pure substrate, the phases P1 and P2, as well as a disordered phase D can be identified. Images (**b**) and (**d**) have been recorded after a small square area (indicated by the *arrow*) has been scanned with much higher frequency shift as usual. During this scan with much higher tip sample interaction, the tip induced an order–disorder transformation. This one can be observed both in the subsequently recorded (**b**) topography and (**d**) KPFM image [81]

the orientation with respect to the surface and the ordering of the molecules which has to be considered to understand the interface dipole layer formation.

11.4 Conclusion

In summary, this chapter described the effects that occur at metal/organic interfaces. In the first part, an overview of the work done by macroscopic methods is given. From an electronic point of view, three different types of contacts can be distinguished: an ohmic contact, a Schottky–Mott contact, or a dipole layer. These effects have been systematically studied by means of macroscopic methods such as the KP, PES, and IPES. KP gives a direct measure for the work function, PES and IPES can be used to estimate the vacuum level (VL) shift relative to the substrate E_f (dipole formation), the ionization potential (IP), the electron affinity (EA), or the position of the LUMO. Macroscopic methods either use the emission of electrons or they rely on well-conducting samples. Thus, for organic layers with reduced conductivity, their application must be done with care. The most important conclusions drawn from macroscopic studies of organic/metal interfaces are the following: Fermi level alignment is not necessarily achieved but rather a dipole layer at the interface is formed, the latter is confined to the very first monolayer only. The size of the dipole layer shows a linear dependence on the metal substrate

work function. The origins for dipolar layer formation can be charge transfer, mirror forces, push back effects, chemical interaction, interface states, permanent dipole of adsorbates, and many more. It is not always the direction of a charge transfer that determines the orientation of the dipole, but rather the redistribution of the electronic cloud. These properties strongly depend on the local environment; therefore, it is crucial to exactly know the geometrical and chemical properties of the investigated interface.

The second part of this chapter is dedicated to the nanoscopic KPFM method. First of all, it is shown that KPFM reveals quantitative values for the local work function. This was demonstrated by comparing locally acquired KPFM values with results from macroscopic methods for a variety of metal/organic (C_{60}) interfaces [54]. Furthermore, some studies were discussed where either the orientation of the adsorbed molecules with respect to the surface or their organization on the surface influenced the measured CPD. The influence of the orientation was demonstrated with the help of two examples. The first was the adsorption of PTCDA on Ag(111) covered by an ultrathin KBr film with a thickness of 1 or 2 ML [69]. It was shown that the CPD observed above differently organized molecules was independent of whether the molecules were adsorbed on the first or the second ML of KBr/Ag(111), but rather depended on the orientation of the molecules with respect to the surface. The second example discussed the adsorption of porphyrin molecules on HOPG [72]. Again, it was found that the CPD strongly depended on the orientation of the adsorbed molecules π-orbital with respect to the surface. The dependence on the molecular arrangement was shown for the case of different structural phases of octachloro zinc phthalocyanine (ZnPcCl8) on Ag(111) [81]. Although these structural phases were assisted by intermolecular hydrogen–halogen bonds (which did not significantly influence their electronic properties), it was primarily the packaging density in these phases which led to the observed work function differences. Besides the packaging density, this study also showed that an order–disorder transformation can vary the local surface potential.

Thus, KPFM is a very versatile tool to characterize metal/organic interfaces. It is indispensable to exactly know the molecular organization and orientation. However, for a complete picture of the complex effects that occur at these interfaces, KPFM must be complemented either with macroscopic methods or with theoretical calculations.

References

1. L. Fu, L. Cao, Y. Liu, D. Zhu, Adv. Coll. Int. Sci. **111**, 133 (2004)
2. H. Ishii, E. Morikawa, S. Tang, D. Yoshimura, E. Ito, K. Okudaira, T. Miyama, S. Hasegawa, P. Sprunger, N. Ueno, K. Seki, V. Saile, J. Electr. Spectrosc. Relat. Phenom. **101–103**, 559564 (1999)
3. L. Buergi, T.J. Richards, R.H. Friend, H. Sirringhaus, J. Appl. Phys. **94**, 6129 (2003)
4. H. Ishii, N. Hayashi, E. Ito, Y. Washizu, K. Sugi, Y. Kimura, M. Niwano, Y. Ouchi, K. Seki, Phys. Status Solidi A **201** (2004)

5. N.F. Mott, Math. Proc. Cambridge Philos. Soc. **34**, 568 (1938)
6. W. Schottky, Phys. Z. **41**, 570 (1940)
7. K. Seki, N. Hayashi, H. Oji, E. Ito, Y. Ouchi, H. Ishii, Thin Solid Films **393**, 298 (2001)
8. T. Leung, C. Kao, W. Su, Phys. Rev. B **68**, 195408 (2003)
9. L. Kelvin, Phil. Mag. **46**, 82 (1898)
10. M. Pfeiffer, K. Leo, N. Karl, J. Appl. Phys. **80**, 6880 (1996)
11. S. Huefner, *Photoelectron Spectroscopy: Principles and Applications Book Description* (Springer, Berlin, 2003)
12. A.M. Ellis, M. Feher, T.G. Wright, *Electronic and Photoelectron Spectroscopy: Fundamentals and Case Studies* (Cambridge University Press, Cambridge, 2005)
13. D.A. Bonnell, R. Shao, Curr. Opin. Solid State Mater. Sci. **7**, 161 (2003)
14. T.W. Kelley, E.L. Granstöm, C.D. Frisbie, Adv. Mater. **11**, 261 (1999)
15. J.R. Matey, J. Blanc, J. Appl. Phys. **57**, 1437 (1985)
16. B.D. Terris, J.E. Stern, D. Rugar, H.J. Mamin, Phys. Rev. Lett. **63**, 2669 (1989)
17. M. Nonnenmacher, M.P. O'Boyle, H.K. Wickramasinghe, Appl. Phys. Lett. **58**(25), 2921 (1991)
18. J.M.R. Weaver, D.W. Abraham, J. Vac. Sci. Technol. B **9**(3), 1559 (1991)
19. H. Ishii, , K. Sugiyama, E. Ito, K. Seki, Adv. Mater. **11**, 605 (1999)
20. N. Hayashi, H. Ishii, Y. Ouchi, K. Seki, J. Appl. Phys. **92**(2), 3784 (2002)
21. H. Peisert, M. Knupfer, J. Fink, Appl. Phys. Lett. **81**, 2400 (2002)
22. H. Peisert, M. Knupfer, T. Schwieger, G. Fuentes, D. Olligs, J. Fink, J. Appl. Phys. **93**, 9683 (2003)
23. I. Campbell, S. Rubin, T. Zawodzinksi, J. Kress, R. Martin, D. Smith, Phys. Rev. B **54**, 14321 (1996)
24. A. Kahn, N. Koch, W. Gao, J. Polymer Sci. Part B: Polymer Phys. **41**, 2529 (2003)
25. N. Venkatamaran, S. Zurcher, A. Rossi, S. Lee, N. Naujoks, D. Spencer, J. Phys. Chem. C **113**, 5620 (2009)
26. H. Mcnally, D. Janes, B. Kasibhatla, C. Kubiak, Superlatt. Microstr. **31**, 239 (2002)
27. J. Lü, E. Delamarche, L. Eng, R. Bennewitz, E. Meyer, H.J. Güntherodt, Langmuir **15**, 8184 (1999)
28. A. Alkauskas, L. Ramoino, S. Schintke, M. von Arx, A. Baratoff, H.J. Güntherodt, T.A. Jung, J. Phys. Chem. B **109**, 23558 (2005)
29. V.D. Renzi, Surf. Sci. **603**, 1518 (2009)
30. R. Balog, P. Cicman, N. Jones, D. Field, Phys. Rev. Lett. **102**, 073003 (2009)
31. E. Ito, Y. Washizu, N. Hayashi, H. Ishii, N. Matsuie, K. Tsuboi, Y. Ouchi, Y. Harima, K. Yamashita, K. Seki, J. Appl. Phys. **92**, 7306 (2002)
32. S. Yanagisawa, K. Lee, Y. Morikawa, J. Chem. Phys. **128**, 244704 (2008)
33. A.K. Henninga, T. Hochwitz, J. Slinkman, J. Never, S. Hoffmann, P. Kaszuba, C. Daghlian, J. Appl. Phys. **77**(5), 1888 (1995)
34. N. Duhayon, P.E.M. Fouchier, T. Clarysse, W. Vandervorst, D. Alvarez, S. Schoemann, M. Ciappa, M. Stangoni, W. Fichtner, P. Formanek, M. Kittler, V. Raineri, F. Giannazzo, D. Goghero, Y. Rosenwaks, R. Shikler, S. Saraf, S. Sadewasser, N. Barreau, T. Glatzel, M. Verheijen, S.A.M. Mentink, M. von Sprekelsen, T. Maltezopoulos, R. Wiesendanger, L. Hellemans, J. Vac. Sci. Technol. B **22**(1), 385 (2004)
35. T. Meoded, R. Shikler, N. Fried, Y. Rosenwaks, Appl. Phys. Lett. **75**(16), 2435 (1999)
36. M. Fujihira, Annu. Rev. Mater. Sci. **29**, 353 (1999)
37. C. Loppacher, U. Zerweck, S. Teich, E. Beyreuther, T. Otto, S. Grafström, L.M. Eng, Nanotechnology **16**, S1 (2005)
38. J. Lü, E. Delamarche, L. Eng, R. Bennewitz, E. Meyer, H.J. Güntherodt, Langmuir **15**, 8184 (1999)
39. H. Sugimura, K. Hayashi, N. Saito, O. Takai, N. Nakagiri, Jpn. J. Appl. Phys. **40**, 4373 (2001)
40. C. Loppacher, U. Zerweck, L.M. Eng, Nanotechnology **15**, S9 (2004)
41. O. Vatel, M. Tanimoto, J. Appl. Phys. **77**(6), 2358 (1995)
42. A. Kikukawa, S. Hosaka, R. Imura, Appl. Phys. Lett. **66**(25), 3510 (1995)

43. I.G. Hill, A. Rajagopal, A. Kahn, Appl. Phys. Lett. **73**(5), 662 (1998)
44. C. Sommerhalter, T. Matthes, T. Glatzel, A. Jäger-Waldau, M.C. Lux-Steiner, Appl. Phys. Lett. **75**(2), 286 (1999)
45. R. Shikler, T. Meoded, N. Fried, Y. Rosenwaks, Appl. Phys. Lett. **74**(20), 2972 (1999)
46. T. Glatzel, D.F. Marrón, T. Schedel-Niedrig, S. Sadewasser, M.C. Lux-Steiner, Appl. Phys. Lett. **81**(11), 2017 (2002)
47. S. Sadewasser, T. Glatzel, M. Rusu, A. Jäger-Waldau, M. Lux-Steiner, Appl. Phys. Lett. **80**(16), 2979 (2002)
48. C.S. Jiang, R. Noufi, J.A. AbuShama, K. Ramanathan, H.R. Moutinho, J. Pankow, M.M. Al-Jassim, Appl. Phys. Lett. **84**(18), 3477 (2004)
49. Y. Leng, C.C. Williams, L.C. Suand, G.B. Stringfellow, Appl. Phys. Lett. **66**(10), 1264 (1995)
50. J. Colchero, A. Gil, A. Berό, Phys. Rev. B **64**, 245403 (2001)
51. U. Zerweck, C. Loppacher, T. Otto, S. Grafström, L.M. Eng, Phys. Rev. B **71**, 125424 (2005)
52. T. Glatzel, L. Zimmerli, S. Koch, B. Such, S. Kawai, E. Meyer, Nanotechnology **20**, 264016 (2009)
53. T. Machleidt, E. Sparrer, D. Kapusi, K.H. Franke, Meas. Sci. Technol. **20**, 084017 (2009)
54. U. Zerweck, C. Loppacher, T. Otto, S. Grafström, L.M. Eng, Nanotechnology **18**, 084006 (2007)
55. J. Lee, Appl. Phys. Lett. **88**, 073512 (2006)
56. M. Nonomura, I. Hiromitsua, S. Tanaka, Appl. Phys. Lett. **88**, 042111 (2006)
57. X. Feng, C. Huang, V. Lui, R. Khangura, Z.H. Lua, Appl. Phys. Lett. **86**, 143511 (2005)
58. I. Horcas, Rev. Sci. Instr. **78**, 013705 (2007)
59. D.R. Linde, *CRC Handbook of Chemistry and Physics* (Boca Raton, FL, 1992)
60. K.D. Tsuei, J.Y. Yuh, C.T. Tzeng, R.Y. Chu, S.C. Chung, K.L. Tsang, Phys. Rev. B **56**, 15412 (1997)
61. C.T. Tzeng, W.S. Lo, J.Y. Yuh, R.Y. Chu, K.D. Tsuei, Phys. Rev. B **61**, 2263 (2000)
62. S. Veenstra, A. Heeres, G. Hadziioannou, G. Sawatzky, H. Jonkman, Appl. Phys. A **75**, 661666 (2002)
63. S.W. Cho, J.H. Seo, C.Y. Kim, K.H. Yoo, K. Jeong, C.N. Whang, Y. Yi, S.J. Kang, M. Noh, Appl. Phys. Lett. **88**, 151103 (2006)
64. X. Cui, M. Freitag, R. Martel, L. Brus, P. Avouris, Nanoletters **3**, 783 (2003)
65. T. Miyazaki, K. Kobayashi, K. Ishida, S. Hotta, T. Horiuchi, H. Yamada, K. Matsushige, Jap. J. Appl. Phys. **42**, 4852 (2003)
66. H. Yamada, T. Fukuma, K. Umeda, K. Kobayashi, K. Matsushige, Appl. Surf. Sci. **188**, 391 (2002)
67. N. Saito, K. hayashi, H. Sugimura, O. Takai, N. Nakagiri, Surf. Interf. Analysis **34**, 601 (2002)
68. V. Palermo, S. Morelli, M. Palma, C. Simpson, F. Nolde, A. Herrmann, K. Mullen, P. Samori, ChemPhysChem **7**, 847 (2006)
69. C. Loppacher, U. Zerweck, L.M. Eng, S. Gemming, G. Seifert, C. Olbrich, K. Morawetz, M. Schreiber, Nanotechnology **17**, 1568 (2006)
70. T. Glatzel, L. Zimmerli, S. Koch, S. Kawai, E. Meyer, Appl. Phys. Lett. **94**, 063303 (2009)
71. L. Ramoino, M. von Arx, S. Schintke, A. Baratoff, H.J. Guntherodt, T. Jung, Chem. Phys. Lett. **417**, 22 (2006)
72. M.P. Nikiforov, U. Zerweck, P. Milde, C. Loppacher, T.H. Park, H.T. Uyeda, M.J. Therien, L. Eng, D. Bonnell, Nano Lett. **8**, 110 (2008)
73. *The Porphyrins*, David Dolphin (Editor), Academic Press, New York, (1978)
74. L. Scudiero, D.E. Barlow, U. Mazur, K.W. Hipps, J. Am. Chem. Soc. **123**, 4073 (2001)
75. L. Scudiero, D.E. Barlow, K.W. Hipps, J. Phys. Chem. B **106**, 996 (2002)
76. H.T. Uyeda, Y. Zhao, K. Wostyn, I. Asselberghs, K. Clays, A. Persoons, M.J. Therien, J. Am. Chem. Soc. **124**, 13806 (2002)
77. J. Otsuki, E. Nagamine, T. Kondo, K. Iwasaki, M. Asakawa, K. Miyake, J. Am. Chem. Soc. **127**, 10400 (2005)
78. T. Terui, T. Kamikado, Y. Okuno, H. Suzuki, S. Mashiko, Curr. Appl. Phys. **4**, 148 (2004)
79. A. Ogunrinde, K. Hipps, L. Scudiero, Langmuir **22**, 5697 (2006)

80. Y. Zhou, B. Wang, M. Zhu, J. Hou, Chem. Phys. Lett. **403**, 140 (2005)
81. P. Milde, U. Zerweck, L. Eng, M. Abel, L. Giovanelli, L. Nony, M. Mossoyan, L. Porte, C. Loppacher, Nanotechnology **19**, 305501 (2008)
82. Z. Bao, A. Lovinger, A. Dodabalapur, Appl. Phys. Lett. **69**, 3066 (1996)
83. B. Crone, A.D.Y.Y. Lin, R. Filas, Z. Bao, A. LaDuca, R. Sarpeshkar, H.E. Katz, W. Li, Nature **403**, 521 (2000)
84. S.R. Forrest, Chem. Rev **97**, 1793 (1997)
85. T. Manaka, M. Iwamoto, Thin Solid Films **438**, 157 (2003)
86. M. Abel, V. Oison, M. Koudia, C. Maurel, C. Katan, L. Porte, ChemPhysChem **7**, 82 (2006)
87. M. Koudia, M. Abel, C. Maurel, A. Bliek, D. Catalin, M. Mossoyan, J. Mossoyan, L. Porte, J. Phys. Chem. B **110**, 10058 (2006)
88. M. Iwamoto, E. Itoh, Thin Solid Films **331**, 15 (1998)
89. D. Sanchez-Portal, P. Ordejon, E. Artacho, J.M. Soler, Int. J. Quantum. Chem. **65**, 543 (1997)
90. J. Soler, E. Artacho, J.D. Gale, A. Garcia, J. Junquera, P. Ordejon, D. Sanchez-Portal, J. Phys. Condens. Matter **14**, 2745 (2002)
91. P. Amsalem, L. Giovanelli, J. Themlin, M. Koudia, M. Abel, V. Oison, Y. Ksari, M. Mossoyan, L. Porte, Surf. Sci. **601**, 4185 (2007)